AGU PUBLICATIONS

JGR

Journal of Geophysical Research: Space Physics

RESEARCH ARTICLE
10.1002/2015JA021508

Key Points:
- Plasma density decay rate in EISCAT observation is too high for neutrals provided by MSIS
- The decay rate was reproduced after the densities of neutrals were modified
- The modified neutral densities reproduced observed plasma density profile without the F_2 maximum

Correspondence to:
D. Sydorenko,
sydorenk@ualberta.ca

Citation:
Sydorenko, D., R. Rankin, and A. W. Yau (2016), Enhanced N_2 and O_2 densities inferred from EISCAT observations of Pc5 waves and associated electron precipitation, *J. Geophys. Res. Space Physics*, *121*, 549–566, doi:10.1002/2015JA021508.

Received 27 MAY 2015
Accepted 7 DEC 2015
Accepted article online 12 DEC 2015
Published online 11 JAN 2016

Enhanced N_2 and O_2 densities inferred from EISCAT observations of Pc5 waves and associated electron precipitation

D. Sydorenko[1], R. Rankin[1], and A. W. Yau[2]

[1]Department of Physics, University of Alberta, Edmonton, Alberta, Canada, [2]Department of Physics and Astronomy, University of Calgary, Calgary, Alberta, Canada

Abstract An advanced two-dimensional numerical model of the coupled ionosphere and magnetosphere is used to analyze EISCAT observations of ULF waves that are accompanied by electron precipitation with a wide energy spectrum. The observations show columns of significantly enhanced electron density produced by pulsating precipitation at altitudes between 150 km and 300 km. After each precipitation pulse, the plasma density returns to its initial value within 2 min. Simulations reveal that such a high-density decay rate cannot be reproduced with the composition of neutrals corresponding to a quiet time provided by the Mass Spectrometer Incoherent Scatter model. To explain the rapid density decay rate using the model of the coupled ionosphere and magnetosphere, the density of nitrogen and oxygen molecules was increased, while the density of oxygen atoms was decreased. The modified neutral densities improved not only the decay rate but also the altitude profile of plasma density which had no F_2 layer maximum before the wave and the pulsating precipitation started.

1. Introduction

Lester et al. [2000] discussed an interesting event observed by the EISCAT Tromsø UHF radar on 21 April 1993 between 0230 and 0450 UT. The present paper focuses on the part of this event from 0320 to 0400 UT. At this time, an intense Pc5 wave with frequency about 5.2 mHz produced temporary enhancements (peaks in the time dependence) of ion temperature with the highest temperature near 1200 K at altitude 212.5 km (the unperturbed ion temperature was about 800 K). The wave also created oscillations of the ion flow velocity between 0 and 1000 m/s in the east-west direction and between −300 and 500 m/s in the north-south direction (altitude 278 km). The wave was identified as an Alfvén wave with azimuthal wave number between 13 and 18 and both torsional and compressional components.

In addition to the wave, there was electron precipitation with a wide energy spectrum and complex time dependence. This included electron beams with energies up to 40 keV that produced a density peak of up to $5 \cdot 10^{11} m^{-3}$ near 100 km altitude and height-integrated Hall conductivity between 20 and 50 mho. Time variations of the high-energy precipitation were rather stochastic and not correlated with the wave.

There was also a second group of much softer electrons, the flux of which was oscillating with the same period as the wave. During each period, substantial ionization by the second group lasted for about 1 min and increased the plasma density at an altitude of 212.5 km from $10^{11} m^{-3}$ to $3 \cdot 10^{11} m^{-3}$. Subsequent to this, the density returned to its original value within about 2 min. The density peak was accompanied by a peak of electron temperature that rises from about 1300 K up to 1800 K and then returns to its initial value. The electron density and temperature peaks almost coincide, with the electron temperature slightly leading. The ion temperature also had one peak per wave period, but the ion temperature was always at its minimum when the electron temperature was maximal and vice versa.

To explain the EISCAT observations, a comprehensive two-dimensional (2-D) model of the coupled ionosphere and magnetosphere [*Sydorenko and Rankin*, 2013] is used below. The model considers propagation of torsional Alfvén waves from the equatorial plane toward the Earth and has good spatial resolution in the *E* and *F* layers of the ionosphere. It includes numerous chemical reactions between ions (H^+, N^+, O^+, N_2^+, NO^+, O_2^+) and neutrals (H, N, O, N_2, NO, O_2), heating and cooling processes for electrons and ions, and a parametric model of electron precipitation. The densities and temperature of neutrals are stationary.

The initial attempt to reproduce observations of *Lester et al.* [2000] using the aforementioned numerical model was unsuccessful. The decay of electron density between precipitation pulses was too slow and the electron density was gradually accumulating. The quasi-stationary vertical electron density profile obtained as an initial condition for the simulations had a distinct F_2 maximum while the profile measured by EISCAT before the event had no such maximum (this was not mentioned in *Lester et al.* [2000]). It is necessary to mention that the International Reference Ionosphere (IRI) model for conditions pertaining to the event described above also gives a density profile with an F_2 maximum. The density accumulation occurs because the dominant neutral species above 200 km is O, and the ion species with the highest rate of production by EUV or precipitation is O^+ which has no direct recombination process except for the dielectronic recombination with a very low rate [*Terao et al.*, 1991]. An important reaction reducing the density of O^+ is

$$O^+ + N_2 \xrightarrow{k_1} NO^+ + N. \quad (1)$$

In its turn, recombination of NO^+

$$NO^+ + e^- \xrightarrow{\alpha_3} N + O \quad (2)$$

is an important process reducing the electron density (coefficients k_1 and α_3 can be found, e.g., in *Blelly et al.* [1996]). While there are many reactions converting other ion species to NO^+, the rate of its recombination at the altitude of observation (212.5 km) is much higher than the rate of its production in reaction (1), which in presence of a large number of O^+ ions makes reaction (1) a bottleneck for the electron density decay. Obviously, increasing the density of N_2 is the most straightforward way to accelerate the decay of O^+ and, correspondingly, the electron density. Alternatively, the coefficient k_1 increases if there is an ion drift relative to neutrals, for example, due to crossed electric and magnetic fields [*Schunk et al.*, 1988]. In the ionosphere, however, this effect is significant only for electric field strengths of the order of 50 mV/m and higher, while the convection electric field in the EISCAT observation is a few times lower, about 20–25 mV/m.

The coefficient also increases for vibrationally excited N_2 [*Pavlov*, 1998]. The enhancement factor (ratio of rates with and without the vibrationally excited molecules) ranges from 1.5 to 5 for altitudes between 150 km and 350 km [*Campbell et al.*, 2006]. The authors, however, found that if one involves the enhancement of k_1 only in order to reproduce the observed plasma density features, the enhancement factor has to be of the order of 30 which is unrealistic, see section 4 below. At the same time, the electron temperature profile observed by EISCAT has significantly lower temperatures at lower altitudes which assumes enhanced energy losses and speaks in favor of higher neutral densities. *Richards* [2002] also concluded that the effect of the vibrational levels on plasma density profile is minor compared to the effect of neutral density modification.

Evidence for enhanced neutral densities in thermosphere has been found in the orbital deceleration of satellites during periods of higher solar activity [*Jacchia*, 1959]. *Prolss and Fricke* [1976] used data from the ESRO 4 satellite and found that during an intense ionospheric storm on 28 and 29 October 1973, the density of nitrogen molecules increased by a factor of more than 25 while the density of helium decreased by a factor of 10 at altitudes near 300 km in the northern auroral zone. It is necessary to mention here that the density changes for the oxygen were small, but the gas analyzer was not distinguishing between the atomic and the molecular oxygen. Further studies of this event showed that the ratio of the densities of N_2 and O increased by a factor of about 10, which reduced the maximum plasma density in the F_2 layer by more than one half [*Prolss*, 1997].

An analytical model of [*Mayr and Volland*, 1972] demonstrated that when a heating source is applied in the *E* layer, at high latitudes the density of N_2 above the heating area goes up while the density of O goes down. This occurs due to an upward wind which grows with altitude faster than the density of O decreases thus creating a diverging flow of O. Note that below 200 km the dominant neutral species is N_2 and the upward wind must ensure the continuity of its flux. In order to achieve this, the wind velocity must grow with the same altitude scale as the N_2 density decays, which is about 2 times smaller than that of O with the same temperature [*Prolss*, 1997].

Mikhailov and Foster [1997] analyzed the disappearance of F_2 layer maximum in the daytime above the Millstone Hill radar during an intense ionospheric storm of 10 April 1990. The event was accompanied by intense Joule heating in strong (up to 100 mV/m) electric fields that produced an exospheric temperature

higher than 2000 K. They found that the anomalously low plasma density can be explained by the increase of the densities of N_2 (by a factor of 3), O_2 (by a factor of 16), and the decrease of the density of O (by a factor of 6). *Richards* [2002] applied a numerical model to study evolution of the altitude and density of F_2 maximum over Australia in September 1974. He also found that in order to reproduce the reduced plasma density during magnetic disturbances on 15 and 16 September one has to increase the density of N_2 and decrease the density of O.

In view of the above and after the first unsuccessful attempt to reproduce the EISCAT observations with neutral parameters provided by Mass Spectrometer Incoherent Scatter (MSIS), the neutral temperature and the densities of O, N_2, and O_2 were modified in the numerical model. A set of parameters was selected which produces the electron density and temperature and the ion temperature very close to the observed values in an altitude range from 100 km to 400 km. The simulation results obtained after these adjustments are described in the present paper.

The paper is organized as follows. In section 2, simulation results with neutral parameters obtained from the MSIS model are discussed. Section 3 is devoted to the simulation with modified neutral parameters which achieved good agreement with the observations. Section 4 discusses the alternative possibility of reproducing the observations by means of enhancement of k_1 due to excitation of vibrational levels of N_2. Section 5 discusses limitations of the model and summarizes the results. Appendix 5 describes the procedure of selection of parameters of the precipitation.

2. Simulation With Neutral Parameters From MSIS-86

The two-dimensional simulations described below were obtained with the following parameters. The simulation area is in the meridional plane and is a rectangle in dipole coordinates. The northern bottom end of the simulation area is at geomagnetic latitude 66.9778°, altitude 121.647 km. The southern bottom end is at geomagnetic latitude 65.2529°, altitude 78.445 km. The corresponding northern and southern top ends are at altitudes 1552.05 km and 1485.46 km, respectively. The structured nonuniform numerical grid has 248 cells along the field lines. In the transverse direction, there are 90 uniform cells in the center and 10 buffer cells with gradually increasing width on each side. The transverse resolution in the central area changes from 917 m at the bottom to 1281 m at the top. The grid size along the central field line changes from 794 m at the bottom to 92716 m at the top.

The model uses dipole coordinates, which means that the bottom boundary of the simulation domain is not parallel to the surface of the Earth. The initial neutral and ion density and temperature profiles are specified along the middle field line, the bottom of which is at 100 km altitude. In the dipole coordinate direction perpendicular to the geomagnetic field (in the meridian plane), values are set equal to those on the middle field line. This places the "effective" bottom of the ionosphere at an altitude of 100 km. Setting the lower boundary below 100 km can lead to numerical instability.

The precipitation model is based on studies by *Maeda and Aikin* [1968] and *Rees* [1969]. The model does not account for ionization by secondary electrons and their propagation away from the point where an ionization event occurs. It also assumes that a secondary electron transfers its energy to ambient electrons locally. Full description of the model is given in [*Sydorenko and Rankin*, 2013]. The expression for the differential electron flux used in the model corresponds to precipitating electrons which are monoenergetic and directed exactly along the field line at the top boundary of the simulation domain. To account for the wide energy spectrum and complex time variation of the precipitation in the observed event, multiple groups of precipitating electrons with different initial energies, energy fluxes, and time dependencies may be combined in the same simulation. The procedure of calculation of parameters of the precipitation groups is given in Appendix 5. It is necessary to mention that the method used in the model can make substantial quantitative errors in ionization profiles for low-energy electron precipitation (below 1 keV), in particular in the altitude and the value of the ionization maximum [*Fang et al.*, 2010]. Thus, the present model is not suitable for high-accuracy quantitative estimates of precipitation parameters. However, this is not the objective of the paper. The main role of the precipitation model here is just to produce a desired altitude profile of ionization and heating, specific values of precipitation energies and energy fluxes are not very important.

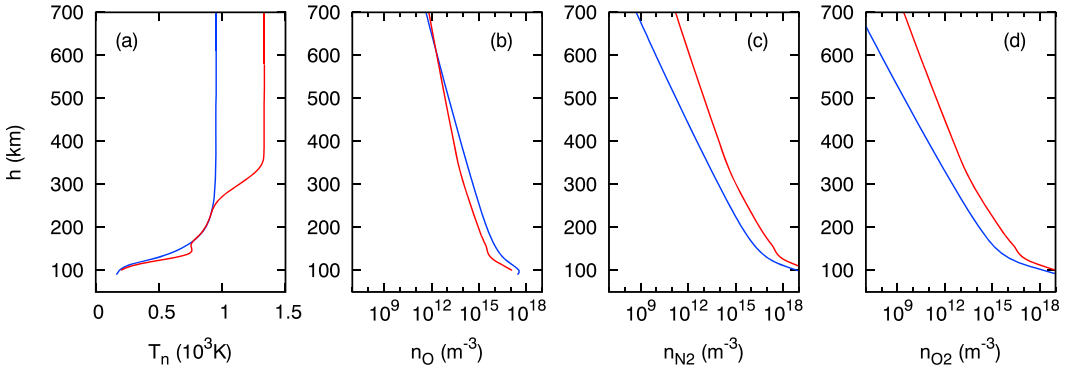

Figure 1. Altitude profiles of (a) neutral temperature and densities of (b) oxygen atoms, (c) nitrogen molecules, and (d) oxygen molecules. Blue curves are provided by MSIS-86 model for 0300 UT, 21 April 1993, geomagnetic latitude 67°, longitude 103° (approximate coordinates of the EISCAT facility in Tromsø). Red curves represent the modified values used in section 3. They are calculated along the center field line of the 2-D simulation area.

2.1. Calculation of Initial Quasi-Stationary State

The procedure of calculation of the initial quasi-stationary state is modified compared to the one described in [*Sydorenko and Rankin*, 2013]. In order to speed up the calculation, a one-dimensional (1-D) version of the model was developed which confines the calculations to the center line of the simulation area and assumes that (i) the initial transverse convection electric field does not change with time and (ii) the transverse gradients are not important. The electric current of ionospheric ions and electrons along the geomagnetic field lines (the parallel direction) cancels the current of precipitating electrons; the latter is a known parameter. This ensures that the total current is divergence free and allows to find the parallel electric field. The 1-D model does not simulate wave propagation, but it updates the parallel electric field (via the extended Ohm's law) and the azimuthal magnetic field (via the Ampere's law) assuming that changes are slow and time derivatives of the fields are unimportant. All ionization and recombination processes, chemical reactions between ions and neutrals, heating and cooling processes, and motion of ions and electrons are in place (though transverse flows do not change density).

The 1-D model is initialized with densities and temperatures of ions and neutrals, electron temperatures, convection electric field, and electron precipitation parameters. Then it runs for a time sufficient to achieve an equilibrium between production and loss of particles and to settle parallel ion flows. The 1-D model produces parallel profiles of ion densities and temperatures and electron temperatures which are used to start the 2-D model with the same transverse electric field, neutral parameters, and electron precipitation parameters. The ionospheric state provided by the 1-D model is so close to a stationary state that it is sufficient to run the 2-D model for only a few tens of seconds to get a 2-D quasi-stationary initial state with fully self-consistent electromagnetic fields and plasma flows. Changes of the electromagnetic fields and plasma parameters introduced at this stage are minimal.

In the simulation results described in this section, the temperature and the density of neutral species are provided by MSIS-86 (A. E. Hedin, Mass Spectrometer Incoherent Scatter (MSIS) neutral atmosphere model, 1987, http://nssdcftp.gsfc.nasa.gov/models/atmospheric/msis/msis86/) for 0300 UT, 21 April 1993, at geomagnetic latitude 67° and longitude 103°, which approximates the position of the EISCAT facility in Tromsø. The neutral parameters are shown by the blue curves in Figure 1. The initial altitude profiles of the ion densities and temperature and the electron temperature are provided by IRI-2007 (IRI, International Reference Ionosphere, 2007, http://nssdcftp.gsfc.nasa.gov/models/ionospheric/iri/iri2007/) for the same time and location as above.

Table 1. Parameters of Electron Precipitation Groups in Simulation With Neutral Parameters From MSIS[a]

Group Number	Initial Energy (keV)	Energy Flux (erg/cm^{2}s)	Type
1	7	10	constant
2	0.5	10	pulsating

[a]The initial energy and flux are defined at the top boundary of the simulation area, for pulsating precipitation the amplitude of the energy flux density is given.

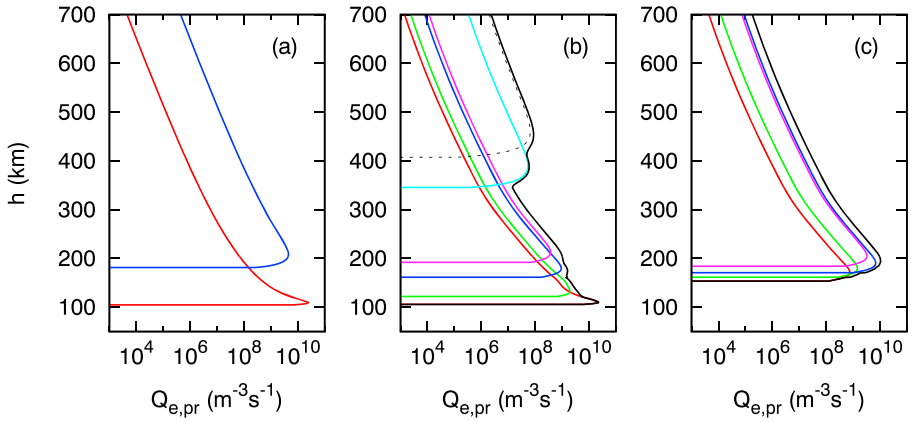

Figure 2. Altitude profiles of total ionization rates (sum over all produced ions) for electron precipitation groups with different initial energy and energy flux in simulation with (a) neutral parameters provided by MSIS and (b, c) with modified neutrals parameters. Figure 2a shows groups of Table 1 with the following colors: group 1 (red) and group 2 (blue). Figure 2b shows the following groups of Table 2: 1 (red), 2 (green), 3 (blue), 4 (magenta), 5 (cyan), and 6 (black dashed); the black solid curve is the sum of ionization rates for all these groups. Figure 2c shows the following groups of Table 2: 7 (red), 8 (green), 9 (blue), and 10 (magenta); the black solid curve is the sum of ionization rates for all these groups. The profiles are calculated along the center field line of the 2-D simulation area.

To get the quasi-stationary initial state, the 1-D model runs for 9592 s, then the 2-D model runs for another 60 s, as described in the previous paragraph. The electron precipitation applied at this stage is represented by group 1 in Table 1. This precipitation is rather energetic and penetrates deep into the ionosphere, the resulting ionization is insignificant above 130 km; see the red curve in Figure 2a. The electron density profile acquires a low-altitude peak which is close to the observed density for altitudes between 105 km and 120 km; compare the blue and the black curves in Figure 3a. A density minimum forms near 190 km. The F_2 layer maximum appears at 279 km altitude which is lower than that of the original IRI profile (green curve in Figure 3a). The height-integrated Pedersen conductivity is 7 mho; see the blue curve in Figure 7h below.

The density maximum consists mostly of O^+ ions; see the unmarked red curve in Figure 4a. For the discussion below it is convenient to have a continuity equation for the O^+ ion density in the following form

$$\frac{\partial}{\partial t} n_{O^+} = Q_{O^+,\mathrm{conv}} + Q^+_{O^+} + Q^-_{O^+}, \tag{3}$$

where $Q_{O^+,\mathrm{conv}}$ combines all terms related to convection,

$$Q^+_{O^+} = Q_{O^+,\mathrm{prec}} + Q_{O^+,\mathrm{EUV}} + k_9 n_O n_{N_2^+} + k_{14} n_{O_2} n_{N^+} + k_{17} n_O n_{N^+} + k_{18} n_O n_{H^+} \tag{4}$$

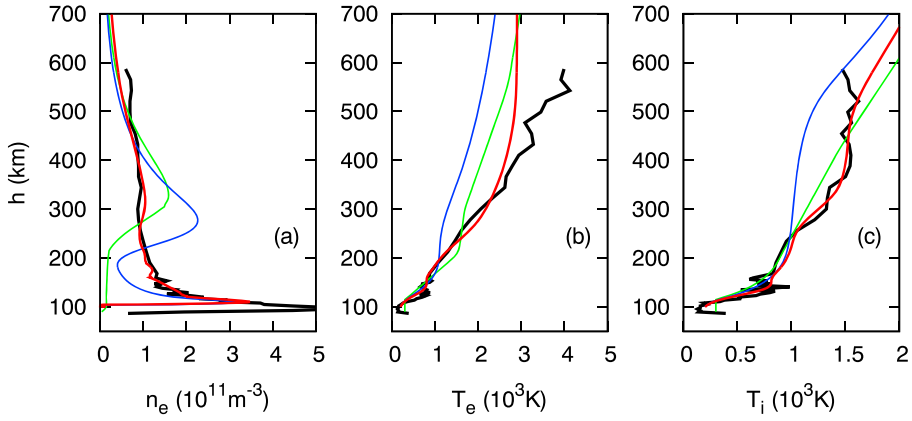

Figure 3. Altitude profiles of (a) electron density, (b) electron temperature, and (c) ion temperature. Black curves are EISCAT Tromsø UHF radar measurements at 0310 UT, 21 April 1993; green curves are obtained from IRI, blue curves represent the quasi-stationary state obtained with original MSIS neutral density and temperature profiles; and the red curves are the quasi-stationary state obtained with modified neutral densities and temperature. Profiles from simulations are calculated along the center field line of the 2-D simulation area.

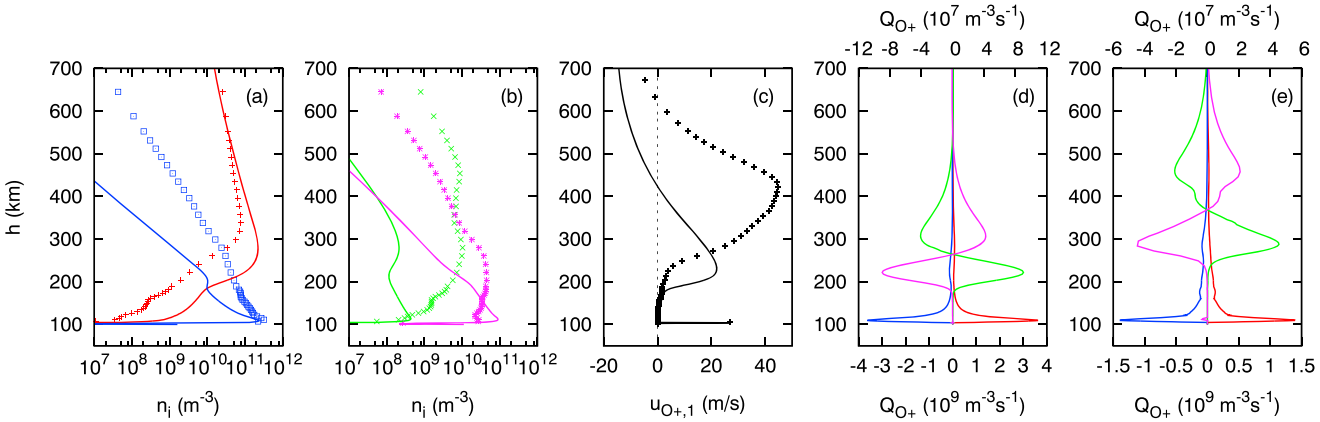

Figure 4. Altitude profiles of the following values. (a) Densities of O^+ (red) and O_2^+ (blue). (b) Densities of N_2^+ (green) and NO^+ (magenta). In Figures 4a and 4b, solid lines are for the simulation with original neutral parameters, markers are for the simulation with modified neutrals. (c) Parallel velocities of O^+ ions in simulation with original (solid black) and modified (black markers) neutral parameters; positive velocities are directed downward. (d) Combined O^+ number density production rate $Q_{O^+}^+$ (red, bottom horizontal axis) and density loss rate $Q_{O^+}^-$ (blue, bottom horizontal axis); sum $Q_{O^+}^+ + Q_{O^+}^-$ (magenta, top horizontal axis) and rate of density change due to convection $Q_{O^+,conv}$ (green, top horizontal axis) in simulation with original neutral parameters. (e) Same as Figure 4d but for the simulation with modified neutrals. The profiles are calculated along the center field line of the 2-D simulation area.

is the combined rate of production of O^+ ions due to electron precipitation $Q_{O^+,prec}$, solar EUV $Q_{O^+,EUV}$, and chemical reactions

$$\begin{aligned} N_2^+ + O &\xrightarrow{k_9} O^+ + N_2, \\ N^+ + O_2 &\xrightarrow{k_{14}} O^+ + NO, \\ N^+ + O &\xrightarrow{k_{17}} O^+ + N, \\ H^+ + O &\xrightarrow{k_{18}} O^+ + H, \end{aligned} \tag{5}$$

and

$$Q_{O^+}^- = -(k_1 n_{N_2} + k_2 n_{O_2} + k_3 n_{NO} + k_4 n_H) n_{O^+} \tag{6}$$

is the combined rate of O^+ ion density loss due to chemical reaction (1) and reactions

$$\begin{aligned} O^+ + O_2 &\xrightarrow{k_2} O_2^+ + O, \\ O^+ + NO &\xrightarrow{k_3} NO^+ + O, \\ O^+ + H &\xrightarrow{k_4} H^+ + O, \end{aligned} \tag{7}$$

coefficients $k_{1-4,9,14,17,18}$ can be found in *Blelly et al.* [1996]. The coefficients $Q_{O^+,conv}$, $Q_{O^+}^+$, and $Q_{O^+}^-$ are defined by equation (8) in *Sydorenko and Rankin* [2013] with terms containing transverse velocity neglected in $Q_{O^+,conv}$.

At the quasi-stationary state, the rates of O^+ production $Q_{O^+}^+$ and loss $Q_{O^+}^-$ balance each other below 180 km; see the red and the blue curves in Figure 4d. At higher altitudes, the difference between the loss and the production $Q_{O^+}^+ + Q_{O^+}^-$ (magenta curve in Figure 4d) is balanced by the convection term $Q_{O^+,conv}$ (green curve in Figure 4d). The convection effect, which reduces density above 280 km while increasing it between 190 km and 280 km, is associated with the O^+ flow directed downward below 420 km (solid black curve in Figure 4c). Without the convection, the maximum should have occurred near 307 km altitude where the difference between the production and loss is maximal; see the magenta curve in Figure 4d. Note that this altitude is close to that of the F_2 maximum predicted by IRI; see the green curve in Figure 3a. The position of the maximum is shifted downward due to the convection by almost 30 km.

The electron and ion temperatures follow the neutral temperature profile in a wide range of altitudes and are significantly lower than the observed values in the areas above 200 km for electrons and above 250 km for ions; compare the blue and the black curves in Figures 3b and 3c.

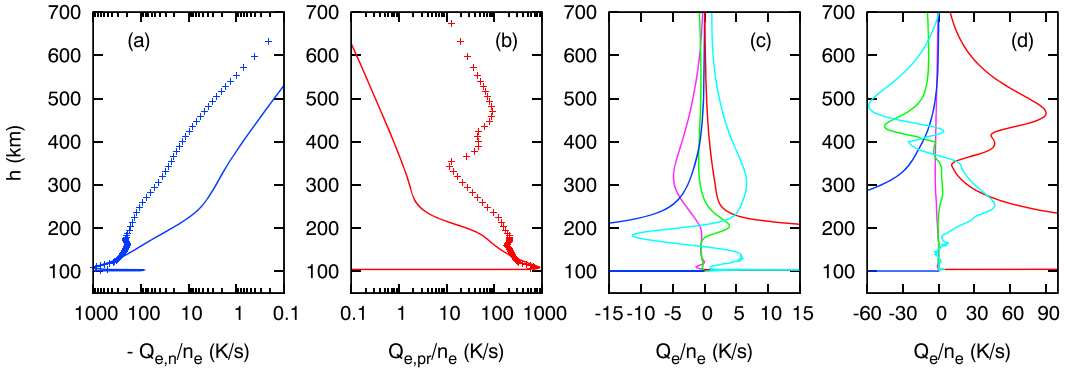

Figure 5. Altitude profiles of the following values. (a) Rates of electron energy loss due to inelastic collisions with neutrals in simulations with the original (solid blue) and modified (blue markers) neutral parameters. (b) Rates of electron heating due to energetic electron precipitation in simulations with the original (solid red) and modified (red markers) neutral parameters. (c) Rates of electron heating by precipitation (red), electron cooling due to inelastic collisions with neutrals (blue), and heat exchange with ions (magenta), electron energy change due to convection and thermoelectric heat flow (green) and thermal conductivity heat flow (cyan) in simulation with original neutral parameters. (d) Same as Figure 5c but for the simulation with modified neutrals. All rates are divided by local values of electron density. The profiles are calculated along the center field line of the 2-D simulation area.

The equation for the electron pressure [*Sydorenko and Rankin*, 2013, equation (15)] can be represented in the following convenient form:

$$\frac{\partial}{\partial t}p_e = Q_{e,\mathrm{conv}} + Q_{e,q} + Q_{e,i} + Q_{e,v} + Q_{e,\mathrm{pr}} + Q_{e,n} + Q_{e,\mathrm{rec}}, \tag{8}$$

where $Q_{e,\mathrm{conv}}$ combines all terms associated with convection, including the thermoelectric heat flow; $Q_{e,q}$ contains the thermal conductivity heat flow; $Q_{e,i}$ describes heat exchange with ions; $Q_{e,v}$ is the frictional heating; $Q_{e,\mathrm{pr}}$ describes heating by electron precipitation; $Q_{e,n}$ is the electron cooling due to inelastic collisions with neutral (excitation of vibrational and rotational levels of N_2 and O_2 and fine structure of O); and $Q_{e,\mathrm{rec}}$ describes losses due to recombination (the last term was not included in *Sydorenko and Rankin* [2013]).

Heating by the precipitation $Q_{e,\mathrm{pr}}$ (unmarked curve in Figure 5b and red curve in Figure 5c) is the dominant heating process for altitudes below 200 km. Here it is balanced by the inelastic collisions with neutrals $Q_{e,n}$ (unmarked curve in Figure 5a and blue curve in Figure 5c). The frictional heating is significant only at very low altitudes (below 120 km). The electron temperature below 250 km is close to the temperature of neutrals; compare the blue curves in Figures 3b and 1a. Terms $Q_{e,\mathrm{pr}}$ and $Q_{e,n}$ become minor above 250 km and 350 km, respectively, other terms ($Q_{e,i}$, $Q_{e,q}$, and $Q_{e,\mathrm{conv}}$) become relatively more important above 250 km but remain small as well (see Figure 5c). The lack of an intense heating source above 250 km results in low-electron temperatures here. Note that one can increase the range of altitudes where the precipitation provides intense heating by including precipitating electrons with lower initial energies, as it is done in section 3, but this will produce additional ionization as well and the electron density profile is already very different from the observed one.

2.2. Two-Dimensional Simulation With Alfvén Wave and Pulsating Precipitation

Initial conditions for this simulation correspond to the quasi-stationary state described in section 2.1. An Alfvén wave with the period of 180 s is excited. The constant energetic electron precipitation (group 1 in Table 1) is still on, and the electron precipitation with lower energy (group 2 in Table 1) with the same period as the wave is applied. The amplitude of the wave and the pulsating precipitation has a bell-shaped profile in the transverse (meridional) direction with the size of about 58 km; see Figure 6. The maximum is shifted northward relative to the center line of the simulation area in order to increase the time it takes for the density perturbation in the *E* layer to reach the southern boundary (this is a potential limit on the duration of the simulation as discussed in *Sydorenko and Rankin* [2013]).

The amplitude of the wave electric field (15 mV/m) is close to the convection electric field, so that the superposition of the two fields bounces between approximately 0 and 30 mV/m; see Figure 7b. This causes oscillations of both the azimuthal ion drift velocity between 0 and about 600 m/s (Figure 7f) and the intensity of the frictional ion heating. In response, the ion temperature produces peaks with amplitude of about 1150 K at times

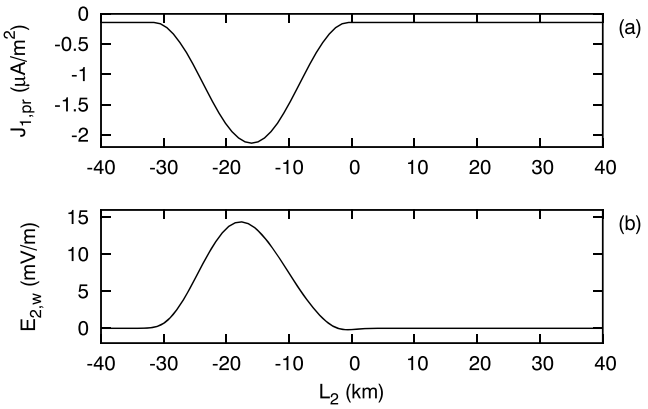

Figure 6. Transverse profiles of (a) the parallel electric current due to the precipitating electrons at time 136.63 s and (b) the meridional wave electric field at time 59.4 s. Both values are near their maximum in time. The altitude at the point of maximum is 534.6 km.

when the total electric field is the strongest; see the blue curve in Figure 7e. The maximal values of the ion temperature and the azimuthal flow velocity are close to those reported in Figure 2b of *Lester et al.* [2000] (1100–1200 K for the temperature and 600–1000 m/s for the azimuthal flow). The meridional ion flow in the simulation is associated mostly with the Pedersen drift since the model considers only torsional azimuthally symmetric Alfvén waves. At the altitude of interest, the meridional drift velocity does not exceed 1 m/s; see the blue curve in Figure 7g. This is a significant difference from the observation where the meridional velocity reached 500 m/s at times.

The phases of oscillations of the electric field and the precipitation flux are adjusted so that the pulse of the precipitation appears when the electric field is at its minimum; compare the blue curve in Figure 7a with the curves in Figure 7b. The precipitation pulses produce correlated spikes in the electron density and temperature. Similar to the observation, a spike of the electron temperature occurs between the two ion temperature spikes; compare the blue curves in Figures 7d and 7e. The maximal electron temperature at the altitude of interest reaches 2800 K, which is about 1000 K higher than the values given in Figure 2b of *Lester et al.* [2000]. Another striking difference is that the electron density decays slowly between the precipitation pulses and the average density gradually grows; see the blue curve in Figure 7c. The density accumulation is associated mostly with O^+ ions; see the blue curve in Figure 8c. The accumulation occurs for H^+ ions as well but the density of this ion species is rather low; see the blue curve in Figure 8a. Other ion species demonstrate sufficiently high decay rate as shown by the blue curves in Figures 8b and 8d–8f.

The data shown in Figure 7 correspond to two altitudes, 213 km and 283 km, similar to the Figure 2b of *Lester et al.* [2000] where altitudes 212.5 km and 278 km were considered. Temporal evolution of electron density and temperature and ion temperature over a wide range of altitudes is shown by color maps in Figure 9. Note that for convenience this figure includes evolution of the drivers as well—the electron precipitation current (Figure 9a) and the meridional electric field (Figure 9b). A similar picture can be downloaded from the EISCAT website. (As of February 2015, in order to download the picture one has to go to http://133.57.20.115/www/cgi-bin/eiscat.cgi or click "Data finder" in http://pc115.seg20.nipr.ac.jp/www/eiscatdata, then select 21 April 1993, time interval 0200–0400 UT, Tromso UHF Radar 2 hours, and click "Submit".) The picture from the website has time resolution about 30–40 s per pixel. An ASCII data file 19930421_uhf0_cp1k_0060.ext can be downloaded at http://pc115.seg20.nipr.ac.jp/www/eiscatdata/tro/ascii/uhf_ascii/1993 as well, but its time resolution is only 2 min.

The main features of the event which one can find in the picture from the website are as follows: (a) the pulsating electron density enhancements stretch from about 150 km to 250–300 km with no density accumulation at any altitude; (b) the electron temperature in the peaks gradually grows with altitude, reaches about 3000 K near 350–400 km, and continues its growth above that altitude; (c) the ion temperature in the peaks reaches about 2000 K at 350 km altitude. For comparison, in the simulation with MSIS neutrals there is a density accumulation between 200 km and 300 km (Figure 9c). The electron temperature in the peaks exceeds 3000 K already at 270 km (Figure 9d) and its growth saturates above 300 km. The ion temperature in the peaks does not exceed 1250 K for altitudes below 450 km (Figure 9e).

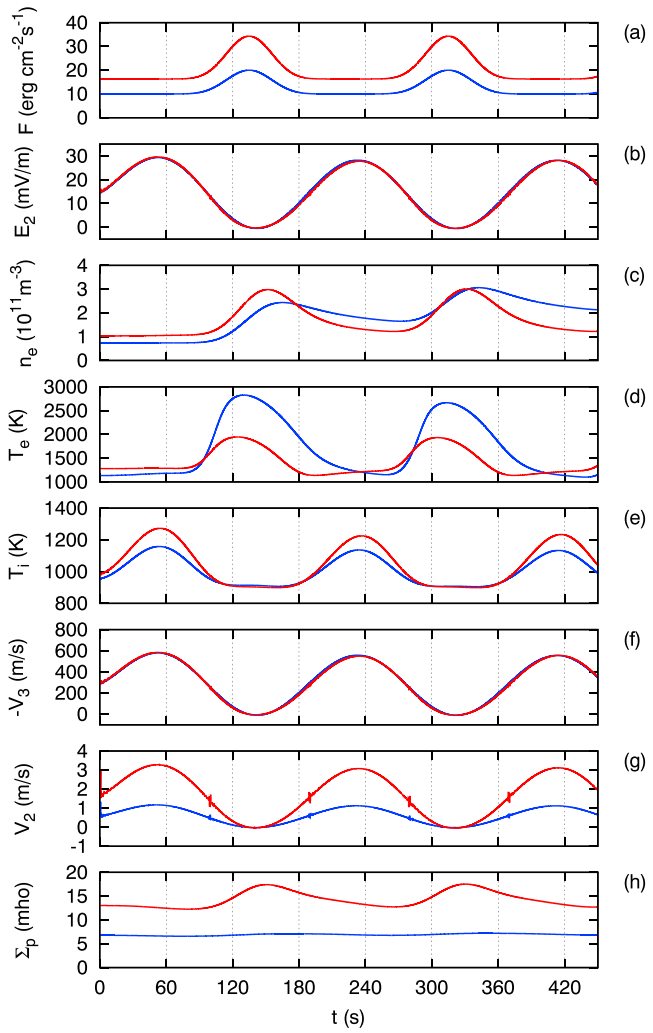

Figure 7. Temporal dependences of (a) electron precipitation energy flux, (b) meridional electric field, (c) electron density, (d) electron temperature, (e) ion temperature, (f) azimuthal and (g) meridional drift velocity of O^+ ions, and (h) height-integrated Pedersen conductivity. The blue curves are for the simulation with neutral parameters from MSIS. The red curves are for the simulation with modified neutral parameters. All values are obtained on the field line where the wave electric field and the precipitating flux are maximal. Values in Figure 7a are at the top of the main simulation area, altitude of 1516 km. Values in Figures 7b, 7f, and 7g are at altitude 283 km. Values in Figures 7c–7e are at altitude 213 km. The positive meridional direction is southward; the positive azimuthal direction is westward. In Figure 7f the sign of the velocity is changed to ensure that the curves look similar to Figure 2 of *Lester et al.* [2000].

3. Simulation With Modified Neutral Parameters

3.1. Neutral Parameters Modification Procedure

Simulation with the original MSIS neutrals described in section 2.2 demonstrated poor agreement with the observation, which is why the neutral parameters were changed as described below. The new parameters were calculated along the central field line of the simulation area which has the altitude of the bottom point 100.17 km. Note that in a 2-D simulation, initial values are defined along the central field line first, then they are distributed without modification across the whole grid in the transverse direction.

As shown by the red curve in Figure 1a, the neutral temperature above 360 km was increased to 1400 K. A smooth transition from the MSIS values was ensured between 280 km and 360 km. Another neutral temperature enhancement for altitudes between 120 km and 160 km was made to mimic similar low-altitude features in the observed electron and ion temperature profiles; see black curves in Figures 3b and 3c. The low-altitude correction has only a minor effect on the processes considered in the paper.

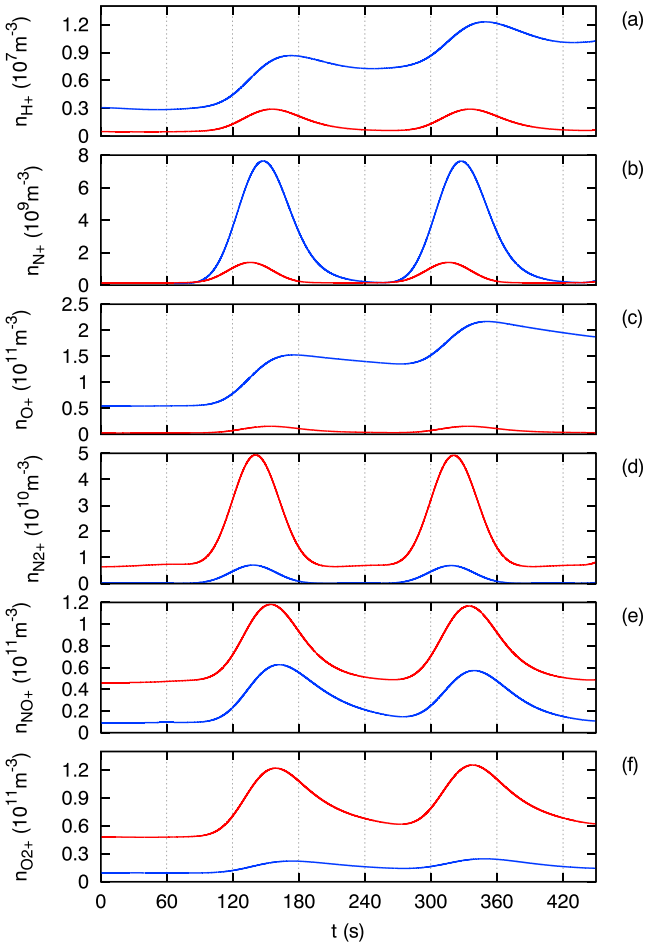

Figure 8. Temporal dependences of number densities of (a) H^+, (b) N^+, (c) O^+, (d) N_2^+, (e) NO^+, and (f) O_2^+ in the simulation with neutral parameters from MSIS (blue) and in the simulation with modified neutral parameters (red). All values are obtained at altitude 213 km on the field line where the wave electric field and the precipitating flux are maximal.

The dynamics of neutrals discussed in *Mayr and Volland* [1972] and *Prolss* [1997] is not included in the model presented in this paper. The altitude profiles of the densities of O, N_2, and O_2 are obtained using an approximate procedure similar to *Richards* [2002]. To obtain the density at altitude h, the following equation assuming diffusive equilibrium was integrated:

$$\frac{\partial}{\partial h}\ln n_\alpha = -\frac{\partial}{\partial h}\ln(k_B T_n) - \frac{m_\alpha g}{k_B T_n}, \tag{9}$$

where T_n is the neutral temperature, g is the acceleration of gravity, k_B is the Boltzmann constant, and n_α and m_α are the density and the mass of neutral species α, $\alpha = O, N_2, O_2$. The integration started at altitude 90 km. The boundary density values for the integration were the MSIS densities at the 90 km altitude multiplied by the following factors: 1.5 (O), 6 (N_2), and 6 (O_2). This approach introduces a minimum number of free parameters defining the final density profile.

This procedure produced neutral densities quite different from the MSIS. Between 150 km and 350 km the density of O reduced by a factor of about 3.5 while the density of N_2 increased by a factor of about 14 and the density of O_2 increased by a factor of about 19 relative to the MSIS values; compare the red and the blue curves in Figures 1b, 1c, and 1d, respectively. Variations of such a scale are significant but not unknown in observations [*Prolss*, 1997]. The values of neutral parameters used here were selected, after several iterations, because they allowed to obtain electron and ion temperatures and electron density close to the observation.

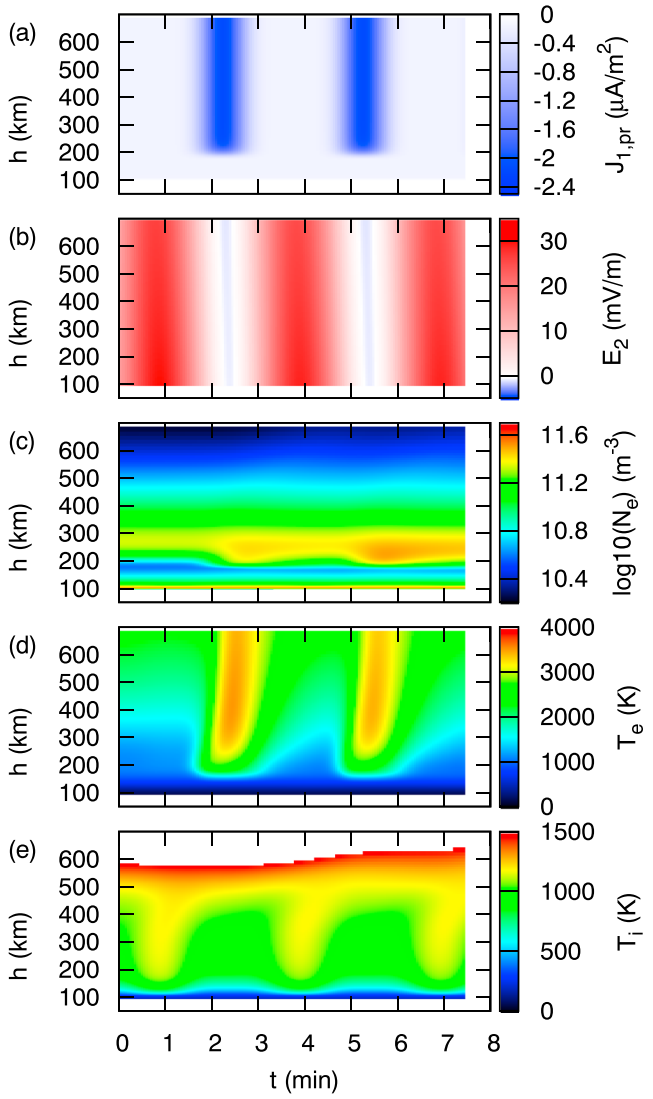

Figure 9. Simulation with neutral parameters from MSIS. (a) Parallel electric current due to electron precipitation, (b) meridional electric field, (c) logarithm of the electron density, (d) electron temperature, and (e) ion temperature as functions of altitude (vertical axis) and time (horizontal axis). All values are obtained along the field line where the wave electric field and the precipitating flux are maximal. The positive parallel direction is downward. The white region above 600 km in Figure 9e appears because the ion temperature here exceeds the upper limit of the color bar.

3.2. Quasi-Stationary State

Calculation of the quasi-stationary state starts with running the 1-D model for 14,388 s (almost 4 h), then the 2-D model runs for another 120 s as described in the beginning of section 2.1. The constant electron precipitation is represented by six groups with a wide range of initial energies (groups 1 to 6 in Table 2). Ionization and energy deposition occur not only in the bottom layers of the ionosphere, but at higher altitudes as well; see Figure 2b. As a result, not only does the low-altitude density peak appear, but a significant amount of plasma is also produced between 140 km and 200 km which eliminates the density depression obtained in the simulation with MSIS neutrals; compare the red and the blue curves in Figure 3a. The dominant ion species here is O_2^+; see blue markers in Figure 4a.

The density profile is very close to the observed one for altitudes between 100 km and 500 km; compare the red and the black curves in Figure 3a. Instead of a pronounced F_2 layer maximum, there is a barely visible density maximum around 340 km. The maximum is still associated with O^+ ions; see the red markers in Figure 4a. Since the density of neutral N_2 and O_2 increased, the area where the loss $Q^-_{O^+}$ of O^+ ions is stronger than the production $Q^+_{O^+}$ and the area where the production is stronger than the loss shifted toward higher altitudes;

Table 2. Parameters of Electron Precipitation Groups in Simulation With Modified Neutrals

Group Number	Initial Energy (keV)	Energy Flux (erg/cm^{2}s)	Type
1	20	10	constant
2	7	2.5	constant
3	2.5	1.3	constant
4	1.3	0.6	constant
5	0.1	0.4	constant
6	0.05	1.5	constant
7	3	1	pulsating
8	2.5	2	pulsating
9	2	10	pulsating
10	1.5	5	pulsating

[a]The initial energy and flux are defined at the top boundary of the simulation area, for pulsating precipitation the amplitude of the energy flux density is given.

compare magenta curves in Figures 4d and 4e. The convection, however, shifts the density maximum downward ($Q_{O^+,conv}$ is the green curve in Figure 4e). Note that although density profiles of O^+, N_2^+, and NO^+ are not monotonically decreasing with altitude (red markers in Figure 4a, green and magenta markers in 4b, respectively) the sum of these densities with the density of O_2^+ (blue markers in Figure 4a) is close to a monotonically decreasing function.

The height-integrated Pedersen conductivity is about 13 mho (red curve in Figure 7h), which is almost twice the value of the conductivity in the simulation with MSIS neutrals (blue curve in Figure 7h). For comparison, *Lester et al.* [2000] reports that the Hall height-integrated conductivity is about 40 mho. Note that the model considers limited range of altitudes and cannot include the lowest parts of the *E* layer for stability reasons.

The multiple electron precipitation groups produce not only intense ionization, but electron heating as well. The rate of electron heating per electron $Q_{e,pr}/n_e$ above 200 km is more than an order of magnitude higher than that in simulation with the MSIS neutral parameters; compare the red markers and the solid red curve in Figure 5b. This heating is balanced by cooling due to inelastic collisions with neutrals up to about 350 km; see the blue markers in Figure 5a and the solid blue curve in Figure 5d. The enhancement of the cooling term $Q_{e,n}$ is partially ensured by the increased neutral densities, but the increase of the electron temperature becomes inevitable as well, which explains the elevated electron temperatures between 200 km and 400 km; compare the red and the blue curves in Figure 3b.

The ion temperature (red curve in Figure 3c) is defined mostly by the balance between frictional heating and heat exchange with neutrals. It follows the neutral temperature (red curve in Figure 1a) up to altitudes of 500 km and is very close to the observed values; compare the red and the black curves in Figure 3c.

3.3. Two-Dimensional Simulation With Alfvén Wave and Pulsating Precipitation

The simulation described here is carried out with the neutrals modified as described in section 3.1 and the initial plasma parameters corresponding to the quasi-stationary state described in section 3.2. An Alfvén wave and a pulsating electron precipitation are applied similar to the simulation with MSIS neutrals in section 2.2. The wave frequency, amplitude, and transverse profile remain essentially unchanged; see Figures 6b and 7b. The transverse profile of the pulsating precipitation flux is qualitatively the same as well, but its amplitude increased in response to the enhanced plasma density decay rate; see the red curve in Figure 7a. The pulsating electron precipitation now consists of four groups (numbered from 7 to 10 in Table 2). This allowed to have maximal ionization near 200 km (the middle of the altitude range for the density enhancements according to the EISCAT data) while producing some ionization as low as 150 km (the bottom of this range); see Figure 2c.

Compared to the simulation with MSIS neutrals, at the altitudes of observation there is virtually no changes in the azimuthal ion flow velocity (Figure 7f) and changes in the ion temperature are small (Figure 7e). However, the ion temperature in the spikes keeps growing up to 400 km where it attains about 1800 K (Figure 10e), which is close to the observed 2000 K ion temperature.

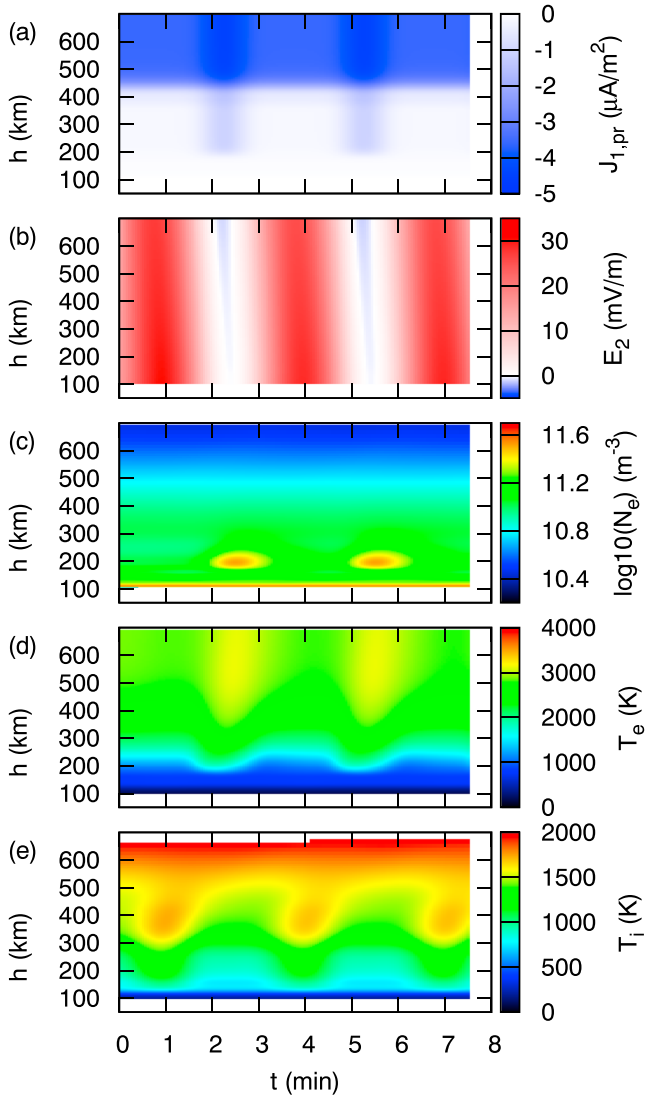

Figure 10. Same as Figure 9 but for the simulation with modified neutrals.

To explain the enhanced ion temperature near 400 km altitude, note first of all that the dominant neutral species at this altitude is N_2 for the modified neutral densities while it is O in the MSIS model. According to equation (5) of *Schunk* [1988] and assuming that frictional heating is balanced by heat exchange with neutrals (for single ion species and single neutral species), the relation between ion temperature and flow velocity is

$$k_B(T_i - T_n) = \frac{m_n}{3m_i} m_i v_i^2 \tag{10}$$

where $T_{i,n}$ and $m_{i,n}$ are the ion and neutral temperatures and masses, respectively, and v_i is the ion flow velocity (the neutrals are considered at rest). The ion flow velocity is defined by the wave electric field and does not change when the neutrals are modified. At 400 km altitude the dominant ion species is O^+ and so the ratio m_n/m_i in the right hand side of (10) is 1 in the MSIS model and 1.75 for the case with modified neutrals, implying an increase in ion temperature.

In spite of the higher precipitation energy flux, the electron temperature in the peaks is almost 1000 K lower than in the simulation with MSIS neutrals because of enhanced losses on inelastic collisions with neutrals; compare the red and the blue curves in Figure 7d. Furthermore, the electron temperature gradually grows with altitude up to 500 km where it attains 3000 K, which gives much better agreement with the observation (3000 K at 350 km) than the simulation with MSIS neutrals; compare Figures 10d and 9d.

Table 3. Parameters of Electron Precipitation Groups in Simulations With Enhanced k_1 and Neutral Parameters From MSIS

Group Number	Initial Energy (keV)	Energy Flux (erg/cm^{2}s)	Type
1	6	10	constant
2	3	3	constant
3	1.5	1	constant
4	0.65	0.5	constant
5	0.5	16	pulsating

[a]The initial energy and flux are defined at the top boundary of the simulation area, for pulsating precipitation the amplitude of the energy flux density is given.

Agreement with the observation is also significantly improved for the plasma density. The precipitation pulses create density enhancements between 150 km and 250 km (between the precipitation pulses there is no density accumulation at any altitude); see the red curve in Figures 7c and 10c. The amplitude of the density peak is about $3 \times 10^{11}\,\mathrm{m}^{-3}$ and is close to the observation. The spikes of the electron temperature are slightly leading relative to the density spikes; compare times when the maxima occur in the red curves in Figures 7c and 7d. This happens when the rate of energy loss due to inelastic collisions with neutrals, which is proportional to the electron density, grows faster than the precipitation energy flux. Note that the plasma density continues its growth for a short time even when the precipitation flux starts decreasing; compare the red curves in Figures 7a and 7c around 140 s. Similar phase difference is present in the observational data as well; compare the two top panels in Figure 2b of *Lester et al.* [2000].

Next, the ion composition of the plasma produced during the precipitation pulses changes significantly. Most of ions produced here are the molecular ions N_2^+ (Figure 8d), NO^+ (Figure 8e), and O_2^+ (Figure 8f). Also, a significant amount of N^+ ions is produced (Figure 8b) although N^+ still remains a minor ion species. The number of O^+ ions is reduced by an order of magnitude (Figure 8c) as well as the number of H^+ ions (Figure 8a). None of the ion species shows signs of accumulation at the altitude of observation.

Finally, the density spikes have clear asymmetry: the growth stage is relatively short and the density-versus-time function $n_e(t)$ is concave down while the decay stage is longer and the $n_e(t)$ function is concave up, see the red curve in Figure 7c. Similar asymmetry is clearly seen in the top panel of Figure 2b of *Lester et al.* [2000]. In the simulation, the shape of $n_e(t)$ at the decay stage is mostly defined by densities of NO^+ and O_2^+ which decrease much slower than the density of N_2^+.

4. Study of the Possible Effect of Vibrational Levels of N_2

The numerical model of *Sydorenko and Rankin* [2013] considers excitation of vibrational levels only as a process of electron cooling. The calculation of the density of vibrationally excited N_2 molecules and the related modification of the coefficient k_1 of reaction (1) is not included. In order to study the effect of the vibrational levels on the plasma density, a set of 1-D simulations was performed where k_1 is multiplied by a constant enhancement factor y. The use of the 1-D model described in section 2.1 is sufficient here because the wave dynamics is much less important for the plasma density than the precipitation, as found in 2-D simulations above. The values of the enhancement factor are in the range from 1 to 31. The neutral parameters are taken from MSIS without modification and the precipitation parameters are in Table 3. The convection electric field and the vertical grid resolution are the same as in the simulations above.

Stationary states calculated *without any electron precipitation* show that the density in the F_2 layer maximum reduces by more than 40% (and approaches the value observed by EISCAT at 300 km) if the enhancement factor is $y = 7$; see Figure 11a. The amplitude of the maximum, however, increases once the electron precipitation is applied. Stationary states calculated *with constant electron precipitation* reveal that in order to obtain the observed density values near 300 km the enhancement factor must be about 30; see Figure 11b. The electron energy losses in the model are not affected directly by the enhancement of k_1 introduced, which is why the electron temperatures for different values of y are similar, see Figure 11c. Note that between 150 km and 250 km altitude, the electron temperatures are significantly higher than the observed values which means that the intensity of cooling is lower than necessary.

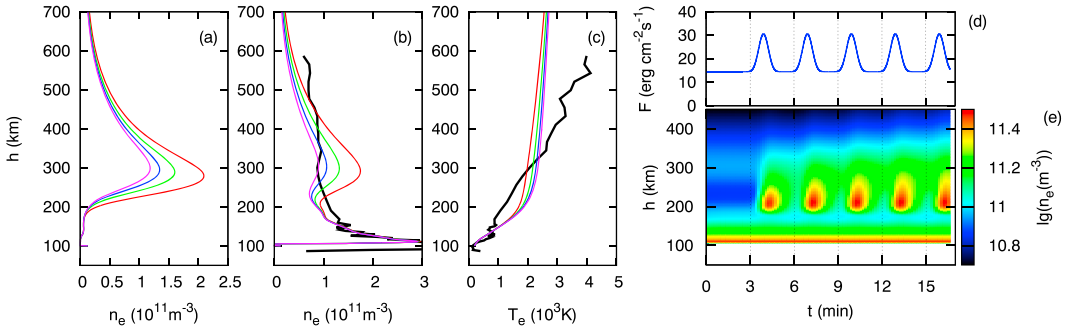

Figure 11. One-dimensional simulations with MSIS neutrals and enhanced coefficient of reaction (1), $k_1' = yk_1$ where $y \geq 1$ is the enhancement factor. (a) Electron density versus altitude in quasi-stationary state without electron precipitation for $y=1$ (red), $y=3$ (green), $y=5$ (blue), and $y=7$ (magenta). (b) Electron density and (c) electron temperature vs altitude in quasi-stationary state with constant electron precipitation for $y=7$ (red), $y=13$ (green), $y=21$ (blue), and $y=31$ (magenta); black curves represent EISCAT data (same as in Figures 3a and 3b). (d) Energy flux of electron precipitation versus time. (e) Logarithm of the electron density versus altitude (vertical axis) and time (horizontal axis). In Figures 11d and 11e, $y=31$. Precipitation parameters are in Table 3. Simulation data curves in Figure 11a and in Figures 11b and 11c are obtained after the system evolved for 8000 and 16,000 s, respectively.

When a pulsating precipitation is applied with $y=31$, the density accumulation is insignificant, similar to the EISCAT observations, though it is slightly more noticeable above 250 km; see Figure 11e. However, such an enhancement factor is half an order of magnitude higher than the maximal enhancement factor of 5 predicted by *Campbell et al.* [2006] below 350 km. Therefore, the enhancement of k_1 by the vibrational levels alone cannot explain the plasma density features in the observed event and must be combined with neutral density modification, which agrees with [*Richards*, 2002].

5. Conclusion

The numerical model of *Sydorenko and Rankin* [2013] is applied to study an intense ionospheric event observed by EISCAT [*Lester et al.*, 2000] where electron precipitation was combined with Alfvén waves in the Pc5 frequency range. The model reproduces the following features of the observation: (i) the anomalously fast rate of plasma density decay, (ii) the altitude plasma density profile without the F_2 layer maximum, (iii) the altitude profiles of the electron and ion temperatures before the event. To achieve this, the neutral temperature is increased, the density of O is decreased, and the densities of N_2 and O_2 are increased. In particular, between 150 km and 350 km the density of O is decreased by a factor of about 3.5, the density of N_2 is increased by a factor of about 14, and the density of O_2 is increased by a factor of about 19 relative to the values provided by MSIS. Similar modifications of neutral densities are indeed observed during periods of magnetospheric disturbances [*Prolss*, 1997] and are the reason for the anomalous dynamics of the F_2 layer maximum [*Mikhailov and Foster*, 1997].

It is necessary to mention that the level of geomagnetic activity in the time of the event is moderate, the planetary index *Kp* for 0000–0300 UT is 4+. However, the event is characterized by intense energetic (tens of keV) and soft electron precipitation and strong currents due to convection electric field which last for hours. The ion density in the *E* layer is very high and consequently so is the frictional heating of neutrals due to the ion flow. In this case, the thermospheric mass density increases locally in the precipitation area [*Zhang et al.*, 2012].

There are several processes which are not included in the model and which may affect the rate of plasma density decay and, correspondingly, the degree of modification of the neutral parameters. First, the coefficient k_1 of reaction (1) increases in the presence of vibrationally excited nitrogen molecules. Such molecules can be obtained in many ways, including direct impact by auroral electrons [see *Campbell et al.* [2006], and references therein]. *Campbell et al.* [2006] estimated the enhancement factor for k_1 during auroras of different intensity and found that it should not exceed 5. Proxy simulations discussed in section 4, however, show that in order to reproduce the observed plasma density properties by increasing the value of k_1 only, the enhancement factor must be near 30. The agreement between the simulation and the observation for the electron temperature is poor in this case.

Second, the plasma density can be reduced due to convection transverse to the geomagnetic field. Near 200 km altitude, the collisions between ions and neutrals are relatively rare and the transverse ion flow is mostly the drift in crossed electric and magnetic fields. The model assumes azimuthal symmetry and considers torsional Alfvén waves in which the transverse electric field is only in the meridional direction. Correspondingly, in simulation the strongest ion drift is in the azimuthal direction and it cannot modify the density due to the symmetry assumption. *Lester et al.* [2000] point out that the wave observed has both compressional and torsional components and corresponds to the azimuthal number in the range between 13 and 18. Such a wave may produce significant flows in both meridional and azimuthal directions, as confirmed by the observation data.

Consider the following two scenarios involving convection. The first scenario is when a periodic density structure created by precipitation periodic in space drifts above an observer who sees variations in time. The second scenario is when the pulsating precipitation source does not move while the transverse convection removes the plasma across the field lines. Since the precipitation pulses and the Alfvén wave have the same frequency, the convection velocity must be equal to the wave phase speed. The azimuthal convection fails to satisfy both scenarios because for the event considered in this paper, the linear azimuthal wavelength is near 900 km and the phase speed about 5 km/s while the azimuthal plasma flow speed does not exceed 1 km/s as shown in Figure 2 of *Lester et al.* [2000]. In the meridional direction, however, the wavelength can be much shorter, which makes the meridional convection associated with the azimuthal electric field a potentially important effect.

While there is no available information about the meridional transverse scale of the observed processes, one can estimate that if the plasma drifts with a velocity of 250 m/s (average meridional drift velocity in Figure 2b of *Lester et al.* [2000] between 0327 UT and 0338 UT) for 100 s, it travels for 25 km. This spatial scale is much larger than the diameter of the spot of the EISCAT beam in the *F* layer which is about 2.8 km [*Uspensky et al.*, 2011]. Therefore, the radar should be able to resolve variations caused by convection with the parameters above.

The present model does not include Hall effects and cannot consider the meridional convection caused by the azimuthal electric field. This limits applicability of the model, however, analysis of Figure 2b of *Lester et al.* [2000] shows that the rapid density decay is not always correlated with significant meridional ion flow velocities. For example, the last density spike in the sequence (near 0354 UT) rapidly disappears while the meridional ion flow velocity does not exceed 100 m/s. Besides, the convection cannot explain the absence of the F_2 layer density maximum which definitely requires the modification of the composition of neutrals. Moreover, in the simulation of the event with the enhanced molecular neutrals, some features of the electron density and temperature closely resemble the observation data: the electron temperature spikes are leading relative to the density spikes and the time dependence of density in the spikes is asymmetric. Another benefit of the enhanced molecular neutral density is that without the enhanced losses due to collisions with neutrals the electron temperature between 150 km and 250 km is much higher than the observed one.

Summarizing, the observed features of the electron density and the electron and ion temperatures are likely due to modification of the temperature and the composition of neutrals in the thermosphere. Amplification of the coefficient k_1 of reaction (1), which can be attributed to the excitation of vibrational levels of N_2, weakly affects the total rate of plasma density decay and cannot be used as a stand-alone explanation. Convection across the geomagnetic field may be an important factor; however, the present model has limited capabilities and does not account for azimuthal variations as well as meridional convection due to the azimuthal electric field. More accurate modeling must combine the effect of vibrationally excited N_2 and the compressional Alfvén waves and describe the dynamics of neutrals (at least at the stage of calculation of the quasi-stationary state) self-consistently.

The precipitation parameters given in Tables 1–3 are selected after a number of test simulations. In other words, one set of parameters is taken, then a test run is made, then the result is compared with the observation data, and the precipitation parameters are appropriately adjusted. This sequence is repeated until the agreement with the observational parameter (usually the plasma density) is reached (at least approximately).

Table 1 describes precipitation parameters for the simulation with MSIS neutrals. The energy of the constant high-energy precipitation in group 1 is adjusted to ensure that the precipitation reaches low-altitude parts of the simulation domain and the flux is selected so that at the stationary stage the low-altitude plasma density peak is on the density-versus-altitude curve plotted with the observation data. One limitation common

in all simulations is that the precipitation cannot reach the very bottom node of the numerical grid—the density here must stay constant for reasons of numerical stability. The energy of soft time-varying precipitation group 2 is selected to ensure maximum ionization at the altitude of the density observation. The flux of this group is adjusted until the value of plasma density in the first spike is reasonably close to the value of $3.6 \times 10^{11} m^{-3}$ reported in *Lester et al.* [2000]. The actual density maximum in the simulation is about 30% lower than in the observation, but in view of the temperature well exceeding the observation, no attempt is made to increase the flux.

Table 2 is for the simulation with modified neutrals. There are six groups with constant precipitation parameters. The procedure of selection applied at the stage of calculation of the quasi-stationary state is as follows. At first, only one group is introduced. The energy of this group is set to a high value similar to group 1 in Table 1 to ensure that the precipitation penetrates as low as possible for the model. Then the flux of this group is adjusted so that the low-altitude part (below approximately 130 km) of the observed density profile (which contains the density peak in the *E* layer) is reproduced. This group is labeled as group 1. Then another group is introduced. The energy of this group is set lower than that of group 1 to ensure that its ionization maximum is at a higher altitude, about 140 km, see the green curve in Figure 2b. This group is labeled as group 2. The flux of group 2 is adjusted to approximate the observed density profile in the vicinity of the maximum of ionization by this group. Then the procedure is repeated for yet another group with even lower energy which is labeled as group 3, and so on. Note that adding a new group with lower energy does not modify the heating and the ionization caused by higher-energy groups below the threshold altitude for the new group.

Table 2 also has four groups of precipitating electrons with pulsating time dependence. The energy of these groups is uniformly distributed between 1.5 keV and 3 keV which expands the altitude range of ionization compared to a monoenergetic precipitation. Several combinations of energy fluxes for these groups are tested. The final set of the fluxes ensures that at the altitude of observation the density value in the maximum of the first density spike is close to the aforementioned value of $3.6 \times 10^{11} m^{-3}$. In the final set, the maximum energy flux is in group 9 while the fluxes in other groups are lower. The combined ionization profile is shown by the black curve in Figure 2c.

Parameters of constant precipitation groups 1 to 4 in Table 3 are selected in a procedure similar to the one used for groups 1 to 6 in Table 2. Parameters of soft time-varying precipitation in group 5 are adjusted to reproduce the maximum of the first density spike similar to group 2 in Table 1.

Acknowledgments
The present study was supported by the Canadian Space Agency (CSA) and the National Sciences and Engineering Research Council of Canada (NSERC). EISCAT is an international association supported by research organizations in China (CRIRP), Finland (SA), Japan (NIPR and STEL), Norway (NFR), Sweden (VR), and the United Kingdom (NERC). The simulation data used to plot the figures in this paper are available upon request from D. Sydorenko (sydorenk@ualberta.ca).

References

Blelly, P. L., A. Robineau, D. Lummerzheim, and J. Lilensten (1996), 8-moment fluid models of the terrestrial high latitude ionosphere between 100 and 3000 km, in *Solar-Terrestrial Energy Program: Handbook of Ionospheric Models*, edited by R. W. Schunk, pp. 53–72, Utah State Univ., Logan, UT and SCOSTEP, Boulder, Colo.

Campbell, L., D. C. Cartwright, M. J. Brunger, and P. J. O. Teubner (2006), Role of electronic excited N_2 and vibrational excitation of the N_2 ground state at high latitudes, *J. Geophys. Res.*, *111*, A09317, doi:10.1029/2005JA011292.

Fang, X., C. E. Randall, D. Lummerzheim, W. Wang, G. Lu, S. C. Solomon, and R. A. Frahm (2010), Parameterization of monoenergetic electron impact ionization, *Geophys. Res. Lett.*, *37*, L22106, doi:10.1029/2010GL045406.

Jacchia, L. G. (1959), Corpuscular radiation and the acceleration of artificial satellites, *Nature*, *183*, 1662–1663.

Lester, M., J. A. Davies, and T. K. Yeoman (2000), The ionospheric response during an interval of Pc5 ULF wave activity, *Ann. Geophys.*, *18*, 257–261.

Maeda, K., and A. C. Aikin (1968), Variations of polar mesospheric oxygen and ozone during auroral events, *Planet. Space Sci.*, *16*, 371–384.

Mayr, H. G., and H. Volland (1972), Magnetic storm effects in the neutral composition, *Planet. Space Sci.*, *20*, 379–393.

Mikhailov, A. V., and J. C. Foster (1997), Daytime thermosphere above Millstone Hill during severe geomagnetic storms, *J. Geophys. Res.*, *102*(A8), 17,275–17,282, doi:10.1029/97JA00879.

Pavlov, A. V. (1998), The role of vibrationally excited oxygen and nitrogen in the ionosphere during the undisturbed and geomagnetic storm period of 6–12 April 1990, *Ann. Geophys.*, *16*, 589–601.

Prolss, G. W. (1997), Magnetic storm associated perturbations of the upper atmosphere, in *Magnetic Storms, Geophys. Monogr.*, vol. 98, edited by B. T. Tsurutani, pp. 227–241, AGU, Washington, D. C.

Prolss, G. W., and K. H. Fricke (1976), Neutral composition changes during a period of increasing magnetic activity, *Planet. Space Sci.*, *24*, 61–67.

Rees, M. H. (1969), Auroral electrons, *Space Sci. Rev.*, *10*, 413–441.

Richards, P. G. (2002), Ion and neutral density variations during ionospheric storms in september 1974: Comparison of measurement and models, *J. Geophys. Res.*, *107*, 1361, doi:10.1029/2002JA009278.

Schunk, R. W. (1988), A mathematical model of the middle and high latitude ionosphere, *Pure Appl. Geophys.*, *127*, 255–303.

Schunk, R. W., W. J. Raitt, and P. M. Banks (1988), Effect of electric fields on the daytime high-latitude E and F regions, *Pure Appl. Geophys.*, *127*, 255–303.

Sydorenko, D., and R. Rankin (2013), Simulation of O^+ upflows created by electron precipitation and Alfvén waves in the ionosphere, *J. Geophys. Res. Space Physics*, *118*, 5562–5578, doi:10.1002/jgra.50531.

Terao, M., K. L. Bell, P. G. Burke, and A. Hibbert (1991), Theoretical study of dielectronic recombination of O^+, *J. Phys. B: At. Mol. Opt. Phys.*, *24*, L321–L326.

Uspensky, M. V., P. Janhunen, A. V. Koustov, and K. Kauristie (2011), Volume cross section of auroral radar backscatter and RMS plasma fluctuations inferred from coherent and incoherent scatter data: A response on backscatter volume parameters, *Ann. Geophys.*, *29*, 1081–1092.

Zhang, B., W. Lotko, O. Brambles, M. Wiltberger, W. Wang, P. Schmitt, and J. Lyon (2012), Enhancement of thermospheric mass density by soft electron precipitation, *Geophys. Res. Lett.*, *39*, L20102, doi:10.1029/2012GL053519.